Dissecting the conformational complexity and flipping mechanism of a prokaryotic heme transporter

Di Wu[1], Ahmad R Mehdipour[2,3], Franziska Finke[1], Hojjat G Goojani[4], Roan R Groh[1], Tamara N Grund[1], Thomas MB Reichhart[1], Rita Zimmermann[1], Sonja Welsch[5], Dirk Bald[4], Mark Shepherd[6], Gerhard Hummer[2,7], Schara Safarian[1,8,9*]

Affiliations

[1] *Department of Molecular Membrane Biology, Max Planck Institute of Biophysics, D-60438 Frankfurt/Main, Germany*

[2] *Department of Theoretical Biophysics, Max Planck Institute of Biophysics, D-60438 Frankfurt/Main, Germany.*

[3] *Center for Molecular Modeling (CMM), Ghent University, Technologiepark 46, Zwijnaarde, 9052 Belgium.*

[4] *Amsterdam Institute for Life and Environment (A-LIFE), AIMMS, Faculty of Science, Vrije Universiteit Amsterdam, 1081 HZ, Amsterdam, The Netherlands*

[5] *Central Electron Microscopy Facility, Max Planck Institute of Biophysics, D-60438 Frankfurt am Main, Germany*

[6] *School of Biosciences, University of Kent, Canterbury CT2 7NJ, United Kingdom*

[7] *Institute of Biophysics, Goethe University Frankfurt, D-60438 Frankfurt/Main, Germany*

[8] *Department of Microbiology and Immunology, School of Biomedical Sciences, University of Otago, Dunedin, NZ-9054, New Zealand.*

[9] *present address: Fraunhofer Institute for Translational Medicine and Pharmacology ITMP Frankfurt, D-60438 Frankfurt/Main, Germany*

*Correspondence and requests for materials should be addressed to Schara Safarian (schara.safarian@biophys.mpg.de).

Abstract

Iron-bound cyclic tetrapyrroles (hemes) are key redox-active cofactors in membrane-integrated oxygen reductases and other bioenergetic enzymes. However, the mechanisms of heme transport and insertion into respiratory chain complexes remain unclear. Here, we used a combination of cellular, biochemical, structural and computational methods to resolve ongoing controversies around the function of the heterodimeric bacterial ABC transporter CydDC. We provide multi-level evidence that CydDC is a heme transporter required for assembly and functional maturation of cytochrome *bd*, a pharmaceutically relevant drug target. Our systematic single-particle cryo-EM approach combined with atomistic molecular dynamics simulations provides detailed insight into the conformational landscape of CydDC during substrate binding and occlusion. Our simulations reveal that heme binds laterally from the membrane space to the transmembrane region of CydDC, enabled by a highly asymmetrical inward-facing CydDC conformation. During the binding process, heme propionates interact with positively charged residues on the surface and later in the substrate-binding pocket of the transporter, causing the heme orientation to flip 180 degrees. The membrane-accessible heme entry site of CydDC is primarily controlled by the conformational plasticity of CydD transmembrane helix 4, the extended cytoplasmic segment of which also couples heme confinement to a rotational movement of the CydC nucleotide-binding domain. Our cryo-EM data highlight that this signal

45 transduction mechanism is necessary to drive conformational transitions toward occluded and
46 outward-facing states.
47
48 **One Sentence Summary:**
49 The heterodimeric bacterial ABC transporter CydDC is a heme flippase essential for the functional
50 maturation of cytochrome *bd*.
51

52 **Introduction**

53 Iron is the second most abundant metal on our planet and an essential trace element for all domains
54 of life (*1–6*). It is involved in a multitude of physiological processes such as photosynthesis, protein
55 biosynthesis, nitrogen fixation, nucleic acid repair, and respiration. Cellular iron is found in the form of
56 iron-sulfur clusters (Fe-S), iron-bound cyclic tetrapyrroles (hemes), or in its free ionic forms. In
57 biological systems, iron mediates electron transfer by acting as electron acceptor or donor in various
58 biochemical reactions (*7*). Terminal respiratory oxidases such as the mitochondrial cytochrome *c*
59 oxidase and the bacterial cytochrome *bd* oxidase are metalloproteins that rely on their redox active
60 heme cofactors for reduction of molecular oxygen to water (*8–14*). Knowledge about the mechanism
61 of maturation and heme insertion of cytochrome *bd*-type oxidases remains unknown but is urgently
62 required for the development of antimicrobial drugs that can specifically target the energy metabolism
63 and respiratory re-wiring of human pathogenic bacteria upon infection and proliferation (*15*, *16*).
64
65 The ABC transporter CydDC is conserved in most bacteria and plays a central role in the biogenesis of
66 membrane-integrated and soluble cytochromes (*17–21*). However, its precise function and molecular
67 mode of action have remained enigmatic for decades (*22*, *23*). CydDC was initially thought to
68 translocate heme across the bacterial cytoplasmic membrane but later studies instead concluded that
69 CydDC is involved in the regulation of the periplasmic redox poise by transporting the reductants
70 glutathione (GSH) and L-cysteine (L-Cys) to the periplasm (*18*, *20*, *24–27*). Despite this widely accepted
71 substrate specificity of CydDC, it was later found that the CydDC complex co-purifies with bound heme
72 (*28*). This observation motivated the assumption that heme represents a prosthetic group of a
73 periplasmic redox sensor domain for regulation of transporter activity (*17*, *22*). A recent work
74 fundamentally challenged the transporter function of CydDC and proposed that it operates as a
75 membrane-bound enzyme catalyzing the reduction of cytoplasmic cystine (CSSC) to L-Cys (*29*).
76
77 To resolve these points of controversy, we used *Escherichia coli* as a model system amenable to our
78 integrative approach including growth-complementation studies, biochemical activity assays,
79 systematic single-particle electron cryo-microscopy (cryo-EM), and atomistic molecular dynamics (MD)
80 simulations to characterize the function of CydDC down to the atomic level and to dissect its molecular
81 mode of action. For our structural biology approach, we established a matrix of sample conditions
82 based on a combination of putative substrate molecules (GSH, GSSG, L-Cys, CSSC, and heme),
83 nucleotides that are either susceptible or resistant to hydrolysis (ATP, ADP, ATP+Vi, and AMP-PNP),
84 and rationally designed mutant variants of CydDC. We determined structures of CydDC under 23
85 different sample conditions at resolutions of 2.7 to 3.9 Å (table S1, and figs. S1 to S7). Based on these

86 results, we conclude that the primary role of CydDC is the transport of heme for functional maturation
87 of cytochrome *bd* oxidases.

88 **Results**
89

90 **CydDC is required for the functional maturation of both cytochrome *bd* isoforms**

91 We carried out growth complementation studies using the *E. coli* mutant strain MB43, which lacks all
92 terminal oxidases and thus shows impaired respiratory activity (*30*). The growth of this strain is poor
93 compared to wild-type controls, but was improved following the introduction of genes encoding
94 cytochromes *bd*-I (p*cydABX*) or *bd*-II (p*appCBX*) (Fig. 1A and fig. S8). Next, we constructed an isogenic
95 deletion mutant of the *cydDC* operon in the genetic background of MB43. This strain, designated
96 MB43Δ*cydDC*, shows an indistinguishable phenotype to MB43 (Fig. 1A). Unlike MB43 however, the
97 growth of MB43Δ*cydDC* was not restored by introducing p*cydABX* or p*appCBX*. A growth-active
98 phenotype of MB43Δ*cydDC* was only achieved by double complementation with p*cydDC* and either
99 p*cydABX* or p*appCBX* (Fig. 1A). Accordingly, UV-Vis spectroscopy revealed that the characteristic
100 fingerprints of cytochrome *bd* cofactors (hemes *b* and *d*) were absent in membrane fractions of MB43
101 and MB43Δ*cydDC* but clearly detected in the growth-restored complementation strains (Fig. 1B) (*30*–
102 *33*).
103
104 Further, we confirmed oxygen reductase activity of membrane fractions from growth-restored MB43
105 and MB43Δ*cydDC* variants (Fig. 1C and fig. S9A). Finally, we used the highly specific inhibitor aurachin
106 D to demonstrate that restored oxygen consumption was due to the activity of cytochrome *bd* variants
107 (Fig. 1C). In summary, growth complementation studies, UV-Vis spectroscopy and oxygen consumption
108 assays confirmed that CydDC is essential for the assembly of both known variants of cytochrome *bd*
109 (Fig. 1F).
110

111 **ATPase activity of CydDC is stimulated by heme**

112 We next tested affinity-purified CydDC for ATPase activity in the presence of various potential
113 substrates using the Malachite green phosphate assay (fig. S1) (*25*, *28*, *29*, *34*). In contrast to previous
114 reports, we found that GSH and L-Cys (and their oxidized counterparts GSSG and CSSC) failed to induce
115 hydrolysis, whereas heme stimulated the ATPase activity of CydDC in a concentration-dependent
116 manner (Fig. 1, D and E, and fig. S10). This effect was only observed for heme itself, but not for its
117 macrocycle scaffold Protoporphyrin IX, or free iron, suggesting that the complexed iron molecule might
118 play a critical role in binding and coordination (Fig. 1D). For verification of our results, we employed a
119 second conceptually different ATP hydrolysis assay based on an enzyme-coupled approach utilizing
120 pyruvate kinase and lactate dehydrogenase (fig. S11A). Both assays confirm the ATPase stimulating
121 effect of heme while showing that the tested reductants do not show typical effects of ABC transporter
122 substrates. To bolster our finding of heme as a primary candidate for a substrate molecule of CydDC,
123 we determined kinetic parameters for heme and ATP. We obtained K_M^{app} and V_{max} values of 79.7 nM

124 and 187.04 nmol [Pi] · nmol [CydDC]$^{-1}$ · min^{-1} for heme, and 91.9 μM and 191.58
125 nmol [Pi] · nmol [CydDC]$^{-1}$ · min^{-1} for ATP (Fig. 1E, and fig. S11, B and C). These values are reasonable
126 regarding the physiological occurrence of both substrates (*35*, *36*).
127
128 Next, we generated glutamate to glutamine mutants of the Walker B domains of CydD and CydC to
129 determine whether CydDC possesses a functionally degenerate nucleotide-binding domain (NBD) as
130 found in other ABC transporters (*37*). In case of the CydD^{E511Q}C mutant, we were not able obtain pure
131 and homogeneous preparations of sufficient yield upon recombinant production. In contrast, the
132 CydDC^{E500Q} mutant was stably purified and did not show any reduction in its T_M as compared to the
133 wild-type variant (fig. S1). Using heme as substrate, we showed that the conserved Walker B glutamate
134 of CydC is essential for ATPase activity of CydDC (Fig. 1D, and figs. S12A and S13). In line with this
135 observed lack of enzymatic activity, transformation of MB43Δ*cydDC* with *pE500Q* (CydDC^{E500Q}) in
136 combination with either p*cydABX* or p*appCBX* did not restore bacterial growth (Fig. 1, A and B, and fig.
137 S9, B and C). We thus conclude that NBD^{C} represents the canonical hydrolysis site and that CydD most
138 presumably contains a degenerate NBD.
139
140 To verify our findings on the role of heme as a potential substrate molecule and to dissect the
141 molecular basis of CydDC function, we employed a systematic single-particle cryo-EM approach for
142 structure determination of CydDC in the presence of different putative substrate molecules,
143 nucleotides, and inhibitors (table S1, and figs. S2 to S7). By solving CydDC structures in biochemically
144 defined states and under turnover conditions, we gained an in-depth view of the conformational
145 landscape and substrate binding modes of this transporter. This allows us to describe key events in
146 substrate recognition, gating, and translocation across the cytoplasmic membrane. In the following,
147 we will focus on the major conformations obtained and their roles in substrate binding, ATP hydrolysis,
148 and substrate release.
149
150 **General architecture of CydDC**
151 The nucleotide and substrate-free, inward-facing conformation of CydDC ($\mathbf{IF}^{\mathrm{apo}}_{\mathrm{as\ isolated}}$), which was
152 obtained in conditions lacking any externally added compounds, exhibits canonical features of type IV
153 ABC transporters (Fig. 2, A and B) (*38–40*). Each subunit is composed of a membrane domain formed
154 by six transmembrane α-helices (TMH), an N-terminal cytoplasmic elbow helix (EL) oriented parallel to
155 the membrane plane, and a cytoplasmic nucleotide-binding domain (Fig. 2, A and B). Both NBDs
156 feature a typical RecA-type fold and two peripheral ABC specific subdomains ABCα and ABCβ (Fig. 2A)
157 (*41*). In this conformation the heterodimer adopts an asymmetrical structure with an overall Cα root-

158 mean-square deviation (RMSD) of 4.17 Å (TMH: 3.28 Å; NBD: 2.5 Å) (fig. S14). Particularly TMs 4 and 5
159 show a pronounced conformational difference between CydD and CydC.
160
161 **Structural insights into substrate specificity**
162 The successful determination of the $\mathbf{IF}^{\text{apo}}_{\text{as isolated}}$ conformation was followed by a systematic screen for
163 substrate molecules that locate within a specific binding pocket. We solved cryo-EM structures of
164 CydDC in the presence of the putative substrate molecules GSH, GSSG, L-Cys, CSSC, and heme
165 individually (Fig. 2C). Distinct densities within the TMH domain were neither obtained in the presence
166 of reduced nor of oxidized forms of glutathione and cysteine. By contrast, we were able to
167 unambiguously identify a bound heme molecule within the TMH domain (fig. S15). This finding is
168 consistent with the ATP hydrolysis inducing effect of heme (Fig. 1D and fig. S11). In addition, we
169 determined structures of CydDC in the presence of a combination of heme and thiols (GSH, GSSG, L-
170 Cys) in order to assess whether these molecules may be heme-dependent co-substrates of CydDC. This
171 possibility was, however, ruled out because we could identify ligand density only for heme but did not
172 observe signal for any other added molecule. It is important to note that we obtained heme bound
173 CydDC conformations not only through exogenous heme addition but consistently also from subsets
174 of CydDC particles that natively co-purified with heme in sample compositions free of external heme
175 (Fig. 2C). This observation further reinforces our working hypothesis that heme is the physiological
176 substrate of CydDC (Fig. 1F).
177
178 **Heme binding and occlusion requires sequential conformational transitions**
179 The binding of heme and the formation of an inward-facing confined state requires distinct
180 conformational changes within the TMH domain of CydDC. From the sum of analyzed sample
181 conditions, we obtained three heme-bound states of CydDC that provide comprehensive insight into
182 this process and allow us to delineate conformational transitions during this process (Figs. 2C and 3,
183 and figs. S15 and S16). Based on these structural insights, we can assign that heme initially binds to a
184 cavity formed by transmembrane helices $TM2^{C}$, $TM3^{C}$, $TM5^{D}$, and $TM6^{D}$ that is in the vicinity of the
185 lateral membrane plane (Fig. 3A, and figs. S15 and S16). In this $\mathbf{IF}^{\text{heme}}_{\text{bound}}$ conformation, which was
186 obtained exclusively under active turnover, the heme molecule primarily interacts with the invariant
187 $H85^{C}$ residue which functions as an axial ligand for the heme iron at a distance of 3.4 Å (Fig. 2C).
188 Additionally, the two heme propionate groups are located in a reasonable distance to form
189 electrostatic interactions with $R81^{C}$ of $TM2^{C}$ and $R136^{C}$ of $TM3^{C}$, respectively (Fig. 3A, figs. S15 and S16,
190 and movie S1). Despite these key interactions, heme is not tightly bound since the distinct density
191 features of the porphyrin macrocycle are less pronounced than the overall local resolution consistent
192 with a dynamically bound substrate (fig. S15). We assign the $\mathbf{IF}^{\text{heme}}_{\text{coordinated}}$ state as the second step in

193 the binding cascade. Here, the interaction between CydDC and heme is strengthened by movement of
194 the C-terminal segment of $TM6^D$ toward the heme and concomitant sidechain rearrangements of
195 $H312^D$, which acts as a second axial ligand of the heme iron (Fe - $H312^D$ distance 2.6 Å), and $Y311^D$,
196 which moves in front of the porphyrin plane and thereby prevents heme from escaping to the
197 membrane space (Fig. 3A, figs. S15 and S16, and movie S2 and S3). The interaction between $TM6^D$ and
198 EL^D further causes positioning of the elbow helix closer towards $TM4^D$, which narrows the membrane
199 accessible gate to the heme binding site (Fig. 3D, figs. S15 and S16, and movie S3). Overall, the TMH
200 region adopts a more compact state upon heme binding and coordination. This compaction is the
201 result of small-scale movements of all transmembrane helices (except $TM4^C$ and $TM5^C$) towards the
202 symmetry axis of the TMH domain (movie S2).
203
204 The most abundant heme-bound conformation obtained (11 individual structures) is termed $\mathbf{IF}^{\mathrm{heme}}_{\mathrm{confined}}$
205 and represents the confined inward-facing TMH conformation (Figs. 2C and 3A). Upon binding and
206 tight coordination of heme, a crucial conformational change of $TM4^D$ is induced (movie S4). Movement
207 of this 7.2 nm long extended transmembrane helix is occurring on two levels (movie S5 and S6). The
208 membrane embedded segment of $TM4^D$ (segment 164-195) changes its angle from ca. 60° to ca. 75°
209 relative to the membrane plane and thus moves in front of the heme, blocking the lateral membrane
210 gate (Fig. 3, B and C). The kinked C-terminal half of $TM4^D$ that is exposed to the cytoplasm
211 concomitantly moves towards EL^D and adopts a conformation that runs diagonally above the bound
212 heme molecule (Fig. 3D). Accordingly, the side chain of $F195^D$ moves in front of the heme and aligns in
213 parallel with the porphyrin plane (Fig 3, A and C, and fig. S16). Together with Y311 of $TM6^D$, these
214 aromatic residues generate π-π stacking interactions with the porphyrin plane of the heme. An
215 electrostatic interaction network formed between EL_D and TM4 further contributes to the formation
216 of a tightly-sealed substrate access gate (Fig. 3, A and C, figs. S16 and S17, and movie S5). As a
217 consequence, the central solvent-filled cavity of the TMH domain changes in size and position (Fig. 3A).
218 The formation of a distinct heme-binding pocket narrows the unoccupied space within the TMH
219 domain and establishes a lateral pathway perpendicular to the membrane plane that ends at the
220 tightly interlocked periplasmic substrate exit gate (Fig. 3A). Furthermore, we observed that even in the
221 absence of any nucleotide, if heme was added to CydDC we exclusively obtained the $\mathbf{IF}^{\mathrm{heme}}_{\mathrm{confined}}$
222 conformation, which provides evidence that binding and confinement of heme occurs independent of
223 nucleotide occupancy of the NBDs (Fig. 2C).
224
225 Based on the deduced sequence of binding events and the distinct interaction patterns between heme
226 and CydDC, we reasoned that the interaction between $H85^C$ and the heme iron marks the most crucial
227 step of substrate recognition and initiation of all subsequent events required to facilitate heme

228 translocation across the membrane. To test this hypothesis, we generated a CydDC H85A[C] mutant
229 (p*H85A*) and performed growth-restoring complementation studies and oxygen consumption
230 measurements using the MB43Δ*cydDC* strain (Fig. 1, A and B, and fig. S9, B and C). In addition, we
231 investigated the effect of the histidine to alanine replacement on ATP hydrolysis activity of CydDC^{H85A}
232 (Fig. 1D). Results of these experiments revealed that lack of this highly conserved histidine residue
233 abrogates the functionality of CydDC (Fig. 1, A, B and D, and figs. S9 and 12B). Furthermore, in contrast
234 to wild-type CydDC, CydDC^{H85A} could not be co-purified with bound heme and could not be loaded by
235 the exogenous addition of heme (fig. S18). These observations were confirmed by cryo-EM structures
236 of CydDC^{H85A}, exclusively adopting the $\mathbf{IF}^{\text{apo}}_{\text{as isolated}}$ conformation, irrespective of presence or absence
237 of exogenously added heme to the samples (Fig. 2C).
238
239 By analyzing the relationship between sample conditions and obtained CydDC conformations we
240 recognized that the $\mathbf{IF}^{\text{heme}}_{\text{coordinated}}$ conformation was obtained only in the presence of the reductants
241 GSH and L-Cys. The fact that their oxidized counterparts do not have a similar effect on CydDC could
242 suggest that the reductive properties of GSH and L-Cys are responsible for stabilizing the
243 $\mathbf{IF}^{\text{heme}}_{\text{coordinated}}$ state. Further, we reason that the systematic absence of $\mathbf{IF}^{\text{heme}}_{\text{confined}}$ state in the presence
244 of GSH and L-Cys together with the consistent observation of $\mathbf{IF}^{\text{heme}}_{\text{coordinated}}$ as the major heme-bound
245 class indicates that these reductants cause opening of the closed lateral heme entry gate. Lack of
246 clearly distinguishable ligand density in the cryo-EM maps of the respective datasets leaves open the
247 question about the precise interaction sites of these thiols and the underlying molecular mechanisms
248 that result in the stabilization of the $\mathbf{IF}^{\text{heme}}_{\text{coordinated}}$ conformation. Further, it remains elusive whether
249 these effects indicate for a physiological link between CydDC function and the two reductants or
250 whether they have to be attributed to the high excess of thiols resulting unspecific reductive effects.
251
252 **MD simulations suggests that heme enters CydDC via the membrane space and is flipped by 180°**
253 To map possible routes of heme entry, we carried out multiple atomistic MD simulations (n=10),
254 focusing on the behavior of heme near lipid bilayer surfaces and the substrate binding pocket of CydDC
255 (Fig. 4 and fig. S19). As a starting point we placed heme near a heterogeneous membrane composed
256 of 70% POPE, 25% POPG and 5% cardiolipin. In 7 out of 10 of our repeated simulations, heme rapidly
257 partitioned into the lipid bilayer, which is consistent with earlier experimental reports about
258 interactions of heme with biomembranes (fig. S19) (*42*, *43*). The porphyrin scaffold immersed deeply
259 into the membrane core and interacted with lipid acyl chains, while the two propionate groups
260 orientated towards the lipid head groups and interacted mostly with the ethanolamine groups of POPE
261 molecules (fig. S19). Next, we analyzed the dynamics of heme placed near the lateral entry site of
262 CydDC in the $\mathbf{IF}^{\text{apo}}_{\text{as isolated}}$ state. Our simulations show that the heme propionates interact with

263 positively charged residues first on the protein surface and then the inside of the binding cavity. These
264 latter interactions induce a rotation of the heme by 90° (Fig. 4). The observation of spontaneous heme
265 binding and rotation suggests this pathway as the primary route for heme entry.
266
267 We carried out further MD simulations using models of $\mathbf{IF}^{\mathrm{heme}}_{\mathrm{bound}}$, $\mathbf{IF}^{\mathrm{heme}}_{\mathrm{coordinated}}$, and $\mathbf{IF}^{\mathrm{heme}}_{\mathrm{confined}}$. When
268 heme is placed within the binding pocket without H85^{C}-Fe coordination, it relaxes toward the entry
269 conformation observed after spontaneous heme binding to $\mathbf{IF}^{\mathrm{apo}}_{\mathrm{as\ isolated}}$ and shows significant mobility
270 within the binding site. However, when heme is axially ligated to H85^{C} in $\mathbf{IF}^{\mathrm{heme}}_{\mathrm{bound}}$, or both H85^{C} and
271 H312^{D} in $\mathbf{IF}^{\mathrm{heme}}_{\mathrm{coordinated}}$ and $\mathbf{IF}^{\mathrm{heme}}_{\mathrm{confined}}$, it maintains the conformation we observed in our cryo-EM
272 structures. We conclude that heme is rotating 90° as it enters the binding site and a further 90° upon
273 binding and axial ligation. This reorientation mechanism may prime heme for directed release toward
274 the periplasmic space or the outer membrane leaflet once the transporter adopts its outward-facing
275 release conformation (Fig. 4).
276
277 These results suggest that CydDC operates via a trap-and-flip mechanism similar to that described for
278 the MFS type proton-dependent lipid transporter LtaA and other primary and secondary active lipid
279 transporters (*44–48*). In MsbA and PfMATE, lipid flipping is primarily driven by electrostatic
280 interactions between lipid head groups and side chains of the respective transporters (*45*, *48*). This
281 functional analogy between lipid and heme flipping indicates that the translocation of amphipathic
282 molecules across biological membranes is presumably based on a common underlying mechanism.
283
284 **Substrate release is ATP dependent but not hydrolysis dependent**
285 Next, we aimed to characterize the mechanistic relationship between substate transport and ATP
286 hydrolysis. Active turnover conditions of wild-type CydDC promote two catalytic states as captured by
287 cryo-EM: $\mathbf{IF}^{\mathrm{heme}}_{\mathrm{bound}}$ and a highly asymmetrical heme-free inward-facing conformation with nucleotide
288 bound to both NBDs ($\mathbf{IF}^{\mathrm{apo}}_{\mathrm{asym}}$) (Fig. 2C). Lack of additional conformations suggests that formation of
289 $\mathbf{IF}^{\mathrm{heme}}_{\mathrm{confined}}$ and subsequent translocation of heme to the periplasmic space via outward-facing
290 conformations occurs rapidly and features short-lived intermediate states. To capture further transient
291 conformations during the transport cycle, we performed an additional turnover cryo-EM experiment
292 using CydDC^{E500Q} that has a significantly reduced hydrolysis activity (Figs. 1 and 2C). This cryo-EM
293 experiment revealed an additional conformation closely matching the TmrAB return state (RMSD =
294 1.32) characterized by Hofmann *et al*. (*49*). Due to the lack of heme in the characterized binding site
295 despite its presence in the sample, we assign this fully occluded conformation as the pre-hydrolysis
296 return state of CydDC ($\mathbf{Occ}^{\mathrm{apo}}_{\mathrm{return}}$) following substrate release (Fig. 3A and fig. S16). In contrast to the
297 turnover dataset of CydDC^{E500Q}, cryo-EM experiments of biochemically defined CydDC^{E500Q} samples

298 revealed conformational heterogeneity reflected by structures of $\mathbf{IF}^{\mathrm{apo}}_{\mathrm{as\ isolated}}$, $\mathbf{IF}^{\mathrm{heme}}_{\mathrm{confined}}$, and
299 $\mathbf{Occ}^{\mathrm{apo}}_{\mathrm{return}}$ states (Fig. 2C). In the presence of heme and ATP (turnover conditions) this heterogeneity
300 becomes resolved by fully driving CydDC^{E500Q} into the $\mathbf{Occ}^{\mathrm{apo}}_{\mathrm{return}}$ state (Fig. 2C). As this effect is not
301 achievable by the addition of heme alone and given the substantially diminished ATPase activity of the
302 CydDC^{E500Q} mutant, we conclude that ATP binding but not its hydrolysis is required for the transition
303 from $\mathbf{IF}^{\mathrm{heme}}_{\mathrm{confined}}$ to $\mathbf{Occ}^{\mathrm{apo}}_{\mathrm{return}}$ state via outward-facing (**OF**) heme-release states (Fig. 1D).

304

305 **Signal transduction and conformational coupling between TMH and NB domains**

306 The transport of heme involves changes in the inter- and intra-subunit symmetry of CydDC. The
307 $\mathbf{IF}^{\mathrm{apo}}_{\mathrm{asym}}$ conformation features the greatest structural asymmetry with an overall Cα RMSD of 5.4 Å
308 (TMH: 3.69 Å; NBD: 1.91 Å) (fig. S14). Loss of symmetry between CydD and CydC in the $\mathbf{IF}^{\mathrm{apo}}_{\mathrm{asym}}$ state is
309 caused by the rotational movement of each subunit along the transporter's central axis perpendicular
310 to the membrane plane (movie S7). In this wedge-like conformation, the distal side (relative to the
311 heme binding domain) of CydDC moves closer together than the proximal half whereby ABCα^{C} and
312 ABCβ^{D} form a semi-interlocked NBD dimer (Fig. 5, A and B, and movie S7). This rearrangement
313 increases the distance between the analogous NBDs of the proximal side, and dilates the heme-
314 accessible membrane cavity (Figs. 3A and 5B). A central question concerning the functionality of ABC
315 transporters is how the information about binding of a substrate molecule to the membrane domain
316 is transduced to the soluble NBDs to induce a fully occluded state for subsequent substrate release
317 and ATP hydrolysis. In CydDC, TM4^{D} has a dual function during the transition from $\mathbf{IF}^{\mathrm{apo}}_{\mathrm{asym}}$ via $\mathbf{IF}^{\mathrm{heme}}_{\mathrm{bound}}$
318 to $\mathbf{IF}^{\mathrm{heme}}_{\mathrm{confined}}$ state. As described above, the membrane-integrated segment of TM4^{D} strongly
319 contributes to sealing the bound heme molecule from the membrane environment (Fig. 3, and figs.
320 S15 and S16). Beyond this function, we found that movement and rearrangement of the cytoplasmic
321 segment of TM4^{D} is associated with a 25° rotation of the horizontal coupling helix 2 (CH2^{D}) connecting
322 TM5^{D} and TM4^{D}. The contact of CH2^{D} with NBD^{C} then establishes a conformational coupling that leads
323 to an almost parallel alignment of the two NBDs, which remain separated by ca. 6-8 Å until ATP is
324 bound to the catalytic nucleotide-binding domain of CydC (Fig. 5A and movie S8).

325

326 **CydDC features a unique nucleotide exchange mechanism**

327 In $\mathbf{IF}^{\mathrm{apo}}_{\mathrm{asym}}$ we discovered a previously unknown mode of interaction between the CydD signature loop
328 and nucleotide bound to the canonical nucleotide-binding site (NBS) of CydC (Fig. 5C). During the
329 asymmetrical interaction of the two NBDs on the distal side, the nucleotide is bound to NBS^{C} and its
330 adenine base is coordinated by Y348^{C} of the A-loop via a π-π interaction on one side, and by a π-cation
331 interaction via R485^{D} of the signature loop from CydD on the opposite side. However, in contrast to

332 previously described fully-interlocked NBD dimers, as for instance from TmrAB[46], the signature loop is
333 separated from the γ-phosphate of the nucleotide by 12.6 Å (Fig. 5C and fig. S20). The degenerate NBS^D
334 has a similar geometry in the $\mathbf{IF}_{\mathrm{asym}}^{\mathrm{apo}}$ state, with the exception that adenine does not participate in π-
335 π stacking and π-cation interactions. This is because of the uncharged $L365^D$ residue at the analogous
336 position of $Y348^C$ in the Walker A motif of CydD, and the fact that the signature loop of CydC is placed
337 at a distance of 20 Å to NBS^D (fig. S20).
338
339 A peculiar and thus far unreported NBS conformation was identified in the $\mathbf{IF}_{\mathrm{confined}}^{\mathrm{heme}}$ state. The
340 conformational coupling between substrate occlusion and signal transduction ($\mathbf{IF}_{\mathrm{asym}}^{\mathrm{apo}}$ to $\mathbf{IF}_{\mathrm{confined}}^{\mathrm{heme}}$) to
341 the NBDs results in the collapse of the NBS^C region and the migration of the Walker A motif into the
342 space originally occupied by the nucleotide phosphate groups (Fig. 5C and movie S9). During this
343 process, the conformation of NBS^D remains mostly unchanged while the signature loop of CydC moves
344 closer towards the nucleotide, although still separated from it by 10 Å. It is noteworthy that in none of
345 the determined $\mathbf{IF}_{\mathrm{confined}}^{\mathrm{heme}}$ structures, we were able to observe nucleotide bound to NBS^C, even in
346 conditions where nucleotide had been added. In contrast, in all cases where externally added
347 nucleotides were present in the sample, a clear density was identified at NBS^D. This observation
348 suggests that the collapsed conformation of NBS^C lacks affinity for the tested nucleotides. A second
349 structural effect of the reductants GSH and L-Cys on CydDC was observed on the level of the NBDs. By
350 a mechanism unknown, both GSH and L-Cys cause stabilization of the distal NBD-NBD interaction and
351 allow for nucleotide binding at NBS^C. While this NBD conformation was otherwise only observed during
352 active turnover, GSH and L-Cys appear to stably induce this NBD state even in the presence of heme
353 which otherwise induces the $\mathbf{IF}_{\mathrm{confined}}^{\mathrm{heme}}$ conformation and causes the dissociation of the NBDs and
354 collapsing of NBS^C.
355
356 Sequence analysis of critical structural motifs required for ATP hydrolysis did not reveal known
357 mutations that would abolish ATP hydrolysis by NBD^D. However, the tightly interlocked conformation
358 of $\mathbf{Occ}_{\mathrm{return}}^{\mathrm{apo}}$ provides structural insights into differences between NBDs that may explain hydrolysis
359 deficiency of NBD^D (Figs. 5C and 6, and figs. S20 and S21). The primary difference between ATP bound
360 NBD^D and NBD^C of this pre-hydrolysis state is the respective distance between the switch histidine and
361 the γ-phosphate of ATP. While $H531^C$ is in close distance (2.9 Å) to act as catalytic acid/base during
362 hydrolysis, $H542^D$ is positioned in a less favorable distance of 4.4 Å to participate in polar interactions
363 (Fig. 5C). In addition to this, the weak coordination of the adenosine base, also found in other
364 heterodimeric ABC transporters, might influence the binding stability of the nucleotide at this position
365 (Figs. 5C and 6, and fig. S20) (*49*). Here, it is important to mention that when we determined the
366 $\mathbf{Occ}_{\mathrm{return}}^{\mathrm{apo}}$ state structure from a sample that did not include exogenously added ATP or AMP-PNP, we

observed lack of bound nucleotide at NBS^D but not at NBS^C (Figs. 2C and 6A). Loss of the NBS^D nucleotide might be possible by the presence of a solvent accessible cavity that remains open towards NBS^D even with interlocked NBDs in this conformation, whereas the tight interaction between the A-loop of CydC and ABCα of CydD forms an enclosed inner environment for ATP around NBS^C (Fig. 6B and fig. S21). Given the hydrolysis deficiency of $CydDC^{E500Q}$ and the associated conformational differences observed between turnover datasets of the wild-type and $CydDC^{E500Q}$ variants, we assign the consistently co-purified nucleotide bound to NBS^C as ATP.

Modelling of outward-facing substrate-release conformations of CydDC

To complement our cryo-EM data, we modeled important but experimentally inaccessible short-lived conformational states during the transition from $\mathbf{IF}^{\mathrm{heme}}_{\mathrm{confined}}$ to $\mathbf{Occ}^{\mathrm{apo}}_{\mathrm{return}}$. Our simulation-based modeling allowed us to construct three transient CydDC conformations representing distinct states of the transport cycle (fig. S22). The $\mathbf{Occ}^{\mathrm{heme}}_{\mathrm{confined}}$ state represents heme-loaded CydDC upon ATP binding with tightly interlocked NBDs. To obtain this conformation, we performed an MD simulation for 400 ns of the fully occluded state of CydDC without heme ($\mathbf{Occ}^{\mathrm{apo}}_{\mathrm{return}}$). Further simulations were carried out to generate the $\mathbf{Occ}^{\mathrm{heme}}_{\mathrm{confined}}$ conformation by inserting heme into the binding site using the slow-growth procedure. After generating the initial model, we performed 300 ns of simulation and analyzed the structural stability by RMSD evolution and conformation dynamics. Our final model shows that the transition from $\mathbf{IF}^{\mathrm{heme}}_{\mathrm{confined}}$ to $\mathbf{Occ}^{\mathrm{heme}}_{\mathrm{confined}}$ entails concentered movements of $TM3^C$ and $TM4^D$. This seals the cytoplasmic gate from solvent access and results in a pseudo-symmetric heterodimer conformation (fig. S22 and movie S10).

Starting from the $\mathbf{Occ}^{\mathrm{heme}}_{\mathrm{confined}}$ and $\mathbf{Occ}^{\mathrm{apo}}_{\mathrm{return}}$ states we obtained two outward-open states ($\mathbf{OF}^{\mathrm{heme}}_{\mathrm{confined}}$ and $\mathbf{OF}^{\mathrm{apo}}$) by performing steered MD simulations on the two periplasmic halves of CydDC. Having generated initial models, we checked the stability and the degree of opening after 300 ns of unrestrained simulations. Our outward facing models suggest that heme is released in a sequential process. First, the periplasmic gate formed by all twelve TMs is opened via separation of two lobes composed of TMs 1-2 of CydC and 4-6 of CydD, and vice versa of TMs 1-2 of CydD and 4-6 of CydC ($\mathbf{OF}^{\mathrm{heme}}_{\mathrm{confined}}$) (fig. S23 and movie S11). These movements cause the lateral cavity next to the heme binding site to enlarge and form an exit pathway. During periplasmic gate-opening we found that the overall interaction of heme with the residues in the binding site remained unchanged. Accordingly, we conclude that substrate release is initiated by retraction of H312 of $TM6^D$ and H85 of $TM2^C$ (figs. S22 and S23, and movie S12). These events most likely change the local affinity and trigger the release towards the periplasmic side of the membrane. The post-release $\mathbf{OF}^{\mathrm{apo}}$ conformation features a narrower periplasmic gate than $\mathbf{OF}^{\mathrm{heme}}_{\mathrm{confined}}$. With the complete closing of the periplasmic

402 gate, the transporter adopts its pre-hydrolysis $\mathbf{Occ}_{\mathrm{return}}^{\mathrm{apo}}$ conformation as observed in the cryo-EM
403 structures of CydDC^{E500Q} (Fig. 2C and fig. S23). In this state, TM6^{D} and TM2^{C} already adopt the $\mathbf{IF}_{\mathrm{asym}}^{\mathrm{apo}}$
404 conformation, which would ensure rapid binding of another heme molecule upon ATP hydrolysis and
405 lateral opening of the substrate entry gate (figs. S22 and S23, and movie S13).
406
407 **Conclusions**
408 The molecular basis of CydDC function has been contested for 30 years. The results from various *in*
409 *vitro* and *in vivo* studies led to conflicting conclusions about its role in bacterial physiology, and its
410 function as a heme transporter was previously ruled out (*20*, *25*, *26*). In this study, we provided
411 evidence that translocation of heme from the cytoplasmic space to the periplasm is the primary
412 function of this ABC transporter.
413
414 Based on our multi-layered approach, we suggest a model for the transport cycle that integrates the
415 results of the employed complementary methods (fig. S24). We assign the ATP-bound $\mathbf{Occ}_{\mathrm{return}}^{\mathrm{apo}}$ state
416 as the starting conformation. We biochemically confirmed that NBD^{C} is essential for the ATPase activity
417 of CydDC (Fig. 1D). In line with this, our structural data indicate that hydrolysis of ATP at this site is
418 required for a mechanochemically-induced return to the substrate-free $\mathbf{IF}_{\mathrm{asym}}^{\mathrm{apo}}$ state (Figs. 3A and 5C,
419 and fig. S16). By this rationale, we assign the densities at NBS^{C} of this post-hydrolysis state obtained
420 from the turnover dataset of CydDC to ADP and Pi (Fig. 5C and fig. S20). We further conclude that
421 heme binding to the TMH domain and ATP to NBD^{C} occurs sequentially rather than simultaneously,
422 given that the binding and occlusion of heme ($\mathbf{IF}_{\mathrm{bound}}^{\mathrm{heme}}$ > $\mathbf{IF}_{\mathrm{coordinated}}^{\mathrm{heme}}$ > $\mathbf{IF}_{\mathrm{confined}}^{\mathrm{heme}}$) is needed to induce
423 dissociation of the distal NBD-NBD interaction, causing NBS^{C} to collapse and release of ADP and Pi
424 (Figs. 3 to 5, and movies S7 to S9). Given the fact that heme binding itself is not sufficient to drive the
425 conformational transition toward the return state conformation but merely results in enrichment of
426 the $\mathbf{IF}_{\mathrm{confined}}^{\mathrm{heme}}$ population, we conclude that binding of ATP to NBS^{C} is essential for the transition to the
427 fully occluded $\mathbf{Occ}_{\mathrm{confined}}^{\mathrm{heme}}$ state. In our simulations, this state is followed by the opening of the
428 extracellular gate, the retraction of TM6^{C}, including the axial heme ligand H312^{D}, to adopt the inward
429 facing conformation of this helix, and the collapsing of the heme binding site ($\mathbf{OF}^{\mathrm{apo}}$) (figs. S22 and
430 S23, and movies S10 to S13). After release of the heme to the periplasmic space, the extracellular gate
431 closes again, reverting back to the $\mathbf{Occ}_{\mathrm{return}}^{\mathrm{apo}}$ conformation. This is in agreement with the observation
432 that under turnover conditions of CydDC^{E500Q} in which heme and ATP are present, we exclusively
433 captured the occluded return state conformation. Notably, this is the sole analyzed condition, that
434 does not result in a heme bound conformation of CydDC. Lack of ATP hydrolysis activity of the
435 CydDC^{E500Q} variant traps the transporter in the post-substrate-release state which suggests that the

436 key role of ATP hydrolysis is to convert CydDC to the $\mathbf{IF}_{\mathrm{asym}}^{\mathrm{apo}}$, as observed in the turnover dataset of
437 CydDC^{wt}.
438
439 The transitional cycle of asymmetrical, symmetry-approaching and pseudo-symmetrical
440 conformations during heme transport is unique to CydDC and highlights the mechanistic possibilities
441 for the specialized substrate transport facilitated by heterodimeric ABC transporters and their diverse
442 conformational space (fig. S25). This and previous structural studies of heme-transporting membrane
443 proteins reveal mechanistic and architectural differences reflecting an evolutionary diversity that may
444 be associated with specific physiological pathways and processes these transporters are involved in
445 (*50*–*54*).
446
447 While we cannot fully exclude the possibility that CydDC might be substrate promiscuous and that the
448 previously suggested substrates GSH and L-Cys might tightly bind to CydDC and induce ATP hydrolysis
449 under conditions not met in this work, we can conclude that the heme-induced ATPase stimulation,
450 the highly specific heme-binding pocket, the abrogation of ATPase activity upon mutation of a key
451 heme-binding residue within the TMH domain, native heme remaining bound to this site after
452 solubilization and extraction of CydDC, and the large-scale conformational responses to addition of
453 external heme all indicate for a primary role as a heme transporter. The structural effects of GSH and
454 L-Cys on CydDC observed in our study further suggest that it may be possible that these reductants
455 could hold a regulatory role for the heme transporter function of CydDC. At present, this latter
456 possibility remains a working hypothesis whose confirmation requires in-depth physiological,
457 biochemical, and structural work.
458
459 Lack of CydDC is associated with extensive changes in bacterial metabolism, including an over-oxidized
460 periplasm and perturbed respiratory activity (*17*). A crucial link is found between CydDC and the
461 bacterial terminal oxygen reductase cytochrome *bd*, which relies on the function of CydDC for the
462 insertion of its heme cofactors and functional maturation. This dependency is also reflected in their
463 genomic organization as in most bacteria the structural genes of cytochrome *bd* and CydDC are
464 operonically encoded in the same gene cluster (*55*). In infection studies, Δ*cydC* mutants of
465 *Mycobacterium tuberculosis and Brucella abortus* displayed diminished survival in mouse models (*56*,
466 *57*). Inactivation of CydDC in *M. tuberculosis* also interfered with bacterial persistence during
467 treatment with the front-line drug isoniazid and caused hypersusceptibility to compounds targeting
468 the mycobacterial cytochrome bc_1 complex, with bioenergetic profiles indistinguishable from
469 cytochrome *bd* knock-out strains (*58*, *59*). Hence, CydDC represents a viable target for the
470 development of antibacterial drugs attacking bacterial respiration on the level of assembly.

While our current work provides evidence on a molecular level for the functional link between the heme transport function of CydDC and functional maturation of bacterial cytochromes, two central questions for future research arise. First, are additional and yet unknown periplasmic proteins involved in the process of cytochrome *bd* assembly and cofactor insertion? A putative candidate for a periplasmic chaperone is the heme-binding protein NikA, which is more abundant in *E. coli* strains overexpressing CydDC (*60*). This co-regulation suggests a functional link between CydDC and NikA. However, given the localization of cytochrome *bd* prosthetic heme groups close to the periplasmic membrane surface, it is also conceivable that CydDC could directly interact with the nascent CydA polypeptide and thus might be actively involved in loading heme cofactors to the catalytic subunit of cytochrome *bd*. A first evidence in favor of this scenario is found in *Francisella tularensis*, where a molecular interaction between CydC and CydA was reported based on co-migration patterns in BN-PAGE experiments (*61*). Second, does CydDC functions as a heme scavenger by shifting the equilibrium of membrane-dissolved heme towards the periplasmic leaflet? As shown in previous experimental studies and our MD simulations, partitioning of heme from the aqueous phase into membranes occurs rapidly. However, the transmembrane movement of heme from one bilayer leaflet to the other occurs very slowly (< 1 s^{-1}) (*42*). The kinetic properties of CydDC suggest that heme translocation occurs at much higher rates, indicating that CydDC can shift the equilibrium of membrane-integrated heme towards the periplasmic leaflet. It remains unclear, whether CydDC releases heme to the periplasmic bilayer leaflet, the periplasmic membrane space, or whether it might deliver it directly to another protein. Based on its flippase function, we infer that CydDC could efficiently release heme towards the periplasmic membrane space because the exiting orientation of the heme macrocycle would readily promote electrostatic interactions between the propionate side chains and the periplasmic lipid head groups upon release.

References and Notes

1. Z. Li, *Heme Biology: The Secret Life of Heme in Regulating Diverse Biological Processes* (World Scientific Publishing Company, 2011).

2. Z. Li, Heme Biology: Heme Acts as A Versatile Signaling Molecule Regulating Diverse Biological Processes (Second Edition) (World Scientific Publishing Company, 2020).

3. P. F. Lindley, Iron in biology: A structural viewpoint. *Rep. Prog. Phys.* **59**, 867-933 (1996).

4. T. Ganz, E. Nemeth, Iron homeostasis in host defence and inflammation. *Nat. Rev. Immunol.* **15**, 500-510 (2015).

5. N. C. Andrews, Iron metabolism: Iron deficiency and iron overload. *Annu. Rev. Genom. Hum. Genet.* **1**, 75-98 (2000).

506 6. S. C. Andrews, A. K. Robinson, F. Rodriguez-Quinones, Bacterial iron homeostasis. *FEMS Microbiol. Rev.* **27**,
507 215-237 (2003).
508 7. M. Lienemann, Molecular mechanisms of electron transfer employed by native proteins and biological-
509 inorganic hybrid systems. *Comput. Struct. Biotechnol. J.* **19**, 206-213 (2020).
510 8. S. Safarian, A. Hahn, D. J. Mills, M. Radloff, M. L. Eisinger, A. Nikolaev, J. Meier-Credo, F. Melin, H. Miyoshi, R.
511 B. Gennis, J. Sakamoto, J. D. Langer, P. Hellwig, W. Kühlbrandt, H. Michel, Active site rearrangement and
512 structural divergence in prokaryotic respiratory oxidases. *Science* **366**, 100-104 (2019).
513 9. S. Safarian, H. K. Opel-Reading, D. Wu, A. R. Mehdipour, K. Hards, L. K. Harold, M. Radloff, I. Stewart, S. Welsch,
514 G. Hummer, G. M. Cook, K. L. Krause, H. Michel, The cryo-EM structure of the bd oxidase from M. tuberculosis
515 reveals a unique structural framework and enables rational drug design to combat TB. *Nat. Commun*. **12**, 5236
516 (2021).
517 10. F. Kolbe, S. Safarian, Ż. Piórek, S. Welsch, H. Müller, H. Michel, Cryo-EM structures of intermediates suggest
518 an alternative catalytic reaction cycle for cytochrome c oxidase. *Nat. Commun*. **12**, 6903 (2021).
519 11. S. Buschmann, E. Warkentin, H. Xie, J. D. Langer, U. Ermler, H. Michel, The Structure of cbb3 Cytochrome
520 Oxidase Provides Insights into Proton Pumping. *Science* **329**, 327-330 (2010).
521 12. J. Abramson, S. Riistama, G. Larsson, A. Jasaitis, M. Svensson-Ek, L. Laakkonen, A. Puustinen, S. Iwata, M.
522 Wikström, The structure of the ubiquinol oxidase from Escherichia coli and its ubiquinone binding site. *Nat.*
523 *Struct. Biol.* **7**, 910-917 (2000).
524 13. T. Soulimane, G. Buse, G. P. Bourenkov, H. D. Bartunik, R. Huber, M. E. Than, Structure and mechanism of the
525 aberrant ba3-cytochrome c oxidase from Thermus thermophilus. *EMBO J.* **19**, 1766-1776 (2000).
526 14. T. N. Grund, M. Radloff, D. Wu, H. G. Goojani, L. F. Witte, W. Joesting, S. Buschmann, H. Mueller, I. Elamri, S.
527 Welsch, H. Schwalbe, H. Michel, D. Bald, S. Safarian, Mechanistic and structural diversity between cytochrome
528 bd isoforms of Escherichia coli. *Proc. Natl. Acad. Sci. U.S.A.* **118**, e2114013118 (2021).
529 15. L. Mascolo, D. Bald, Cytochrome bd in Mycobacterium tuberculosis: A respiratory chain protein involved in
530 the defense against antibacterials. *Prog. Biophys. Mol. Biol.* **152**, 55-63 (2020).
531 16. D. Bald, C. Villellas, P. Lu, A. Koul, Targeting Energy Metabolism in Mycobacterium tuberculosis, a New
532 Paradigm in Antimycobacterial Drug Discovery. *MBio* **8**, 159 (2017).
533 17. L. V. Holyoake, R. K. Poole, M. Shepherd, The CydDC Family of Transporters and Their Roles in Oxidase
534 Assembly and Homeostasis. *Adv. Microb. Physiol.* **66**, 1-53 (2015).
535 18. R. K. Poole, F. GIBSON, G. H. Wu, The Cydd Gene-Product, Component of a Heterodimeric Abc Transporter,
536 Is Required for Assembly of Periplasmic Cytochrome-C and of Cytochrome-Bd in Escherichia-Coli. *FEMS*
537 *Microbiol. Lett.* **117**, 217-224 (1994).
538 19. B. S. Goldman, K. K. Gabbert, R. G. Kranz, Use of heme reporters for studies of cytochrome biosynthesis and
539 heme transport. *J. Bacteriol.* **178**, 6338-6347 (1996).
540 20. C. D. Georgiou, H. Fang, R. B. Gennis, Identification of the cydC locus required for expression of the functional
541 form of the cytochrome d terminal oxidase complex in Escherichia coli. *J. Bacteriol.* **169**, 2107-2112 (1987).
542 21. K. J. Bebbington, H. D. Williams, Investigation of the Role of the Cydd Gene-Product in Production of a
543 Functional Cytochrome-D Oxidase in Escherichia-Coli. *FEMS Microbiol. Lett.* **112**, 19-24 (1993).

544 22. M. Shepherd, The CydDC ABC transporter of Escherichia coli : new roles for a reductant efflux pump. *Biochem.*
545 *Soc. T*. **43**, 908–912 (2015).
546 23. R. K. Poole, L. Hatch, M. W. J. Cleeter, F. Gibson, G. B. Cox, G. Wu, Cytochrome bd biosynthesis in Escherichia
547 coli: the sequences of the cydC and cydD genes suggest that they encode the components of an ABC membrane
548 transporter. *Mol. Microbiol.* **10**, 421-430 (1993).
549 24. M. S. Pittman, H. C. Robinson, R. K. Poole, A bacterial glutathione transporter (Escherichia coli CydDC) exports
550 reductant to the periplasm. *J. Biol. Chem.* **280**, 32254-32261 (2005).
551 25. M. S. Pittman, H. Corker, G. H. Wu, M. B. Binet, A. Moir, R. K. Poole, Cysteine is exported from the Escherichia
552 coli cytoplasm by CydDC, an ATP-binding cassette-type transporter required for cytochrome assembly. *J. Biol.*
553 *Chem.* **277**, 49841-49849 (2002).
554 26. B. S. Goldman, K. K. Gabbert, R. G. Kranz, The temperature-sensitive growth and survival phenotypes of
555 Escherichia coli cydDC and cydAB strains are due to deficiencies in cytochrome bd and are corrected by
556 exogenous catalase and reducing agents. *J. Bacteriol.* **178**, 6348-6351 (1996).
557 27. L. V. Holyoake, S. Hunt, G. Sanguinetti, G. M. Cook, M. J. Howard, M. L. Rowe, R. K. Poole, M. Shepherd,
558 CydDC-mediated reductant export in Escherichia coli controls the transcriptional wiring of energy metabolism
559 and combats nitrosative stress. *Biochem. J.* **473**, 693-701 (2016).
560 28. M. Yamashita, M. Shepherd, W. I. Booth, H. Xie, V. Postis, Y. Nyathi, S. B. Tzokov, R. K. Poole, S. A. Baldwin, P.
561 A. Bullough, Structure and Function of the Bacterial Heterodimeric ABC Transporter CydDC: Stimulation of
562 ATPase activity by thiol and heme compounds. *J. Biol. Chem.* **289**, 23177-23188 (2014).
563 29. A. Mironov, T. Seregina, K. Shatalin, M. Nagornykh, R. Shakulov, E. Nudler, CydDC functions as a cytoplasmic
564 cystine reductase to sensitize Escherichia coli to oxidative stress and aminoglycosides. *Proc. Natl. Acad. Sci. U.S.A.*
565 **117**, 23565-23570 (2020).
566 30. H. G. Goojani, J. Konings, H. Hakvoort, S. Hong, R. B. Gennis, J. Sakamoto, H. Lill, D. Bald, The carboxy-terminal
567 insert in the Q-loop is needed for functionality of Escherichia coli cytochrome bd-I. *Biochim. Biophys. Acta -*
568 *Bioenerg.* **1861**, 148175 (2020).
569 31. A. M. Arutyunyan, J. Sakamoto, M. Inadome, Y. Kabashima, V. B. Borisov, Optical and magneto-optical activity
570 of cytochrome bd from Geobacillus thermodenitrificans. *Biochim. Biophys. Acta - Bioenerg.* **1817**, 2087-2094
571 (2012).
572 32. A. Grauel, J. Kägi, T. Rasmussen, I. Makarchuk, S. Oppermann, A. F. A. Moumbock, D. Wohlwend, R. Müller,
573 F. Melin, S. Günther, P. Hellwig, B. Böttcher, T. Friedrich, Structure of Escherichia coli cytochrome bd-II type
574 oxidase with bound aurachin D. *Nat. Commun*. **12**, 6498 (2021).
575 33. A. Theßeling, T. Rasmussen, S. Burschel, D. Wohlwend, J. Kägi, R. Müller, B. Böttcher, T. Friedrich, Homologous
576 bd oxidases share the same architecture but differ in mechanism. *Nat. Commun.* **10**, 1-7 (2019).
577 34. H. Cruz-Ramos, G. M. Cook, G. Wu, M. W. Cleeter, R. K. Poole, Membrane topology and mutational analysis
578 of Escherichia coli CydDC, an ABC-type cysteine exporter required for cytochrome assembly. *Microbiology* **150**,
579 3415–3427 (2004).
580 35. R. Mempin, H. Tran, C. Chen, H. Gong, K. K. Ho, S. Lu, Release of extracellular ATP by bacteria during growth.
581 *BMC Microbiol*. **13**, 301 (2013).

582 36. C. L. Nobles, J. R. Clark, S. I. Green, A. W. Maresso, A dual component heme biosensor that integrates heme
583 transport and synthesis in bacteria. *J. Microbiol. Methods* **118**, 7–17 (2015).
584 37. T. Stockner, R. Gradisch, L. Schmitt, The role of the degenerate nucleotide binding site in type I ABC exporters.
585 *FEBS Lett*. **594**, 3815–3838 (2020).
586 38. C. Thomas, S. G. Aller, K. Beis, E. P. Carpenter, G. Chang, L. Chen, E. Dassa, M. Dean, F. D. V. Hoa, D. Ekiert, R.
587 Ford, R. Gaudet, X. Gong, I. B. Holland, Y. Huang, D. K. Kahne, H. Kato, V. Koronakis, C. M. Koth, Y. Lee, O.
588 Lewinson, R. Lill, E. Martinoia, S. Murakami, H. W. Pinkett, B. Poolman, D. Rosenbaum, B. Sarkadi, L. Schmitt, E.
589 Schneider, Y. Shi, S. Shyng, D. J. Slotboom, E. Tajkhorshid, D. P. Tieleman, K. Ueda, A. Váradi, P. Wen, N. Yan, P.
590 Zhang, H. Zheng, J. Zimmer, R. Tampé, Structural and functional diversity calls for a new classification of ABC
591 transporters. *FEBS Lett*. **594**, 3767–3775 (2020).
592 39. M. Hohl, C. Briand, M. G. Grütter, M. A. Seeger, Crystal structure of a heterodimeric ABC transporter in its
593 inward-facing conformation. *Nat. Struct. Mol. Biol*. **25**, 395–402 (2012).
594 40. A. Noell, C. Thomas, V. Herbring, T. Zollmann, K. Bartha, A. R. Mehdipour, T. M. Tomasiak, S. Bruechert, B.
595 Joseph, R. Abele, V. Olieric, M. Wang, K. Diederichs, G. Hummer, R. M. Stroud, K. M. Pos, R. Tampe, Crystal
596 structure and mechanistic basis of a functional homolog of the antigen transporter TAP. *Proc. Natl. Acad. Sci.*
597 *U.S.A.* **114**, E438-447 (2017).
598 41. C. Oswald, I. B. Holland, L. Schmitt, The motor domains of ABC-transporters. *Naunyn Schmiedebergs Arch.*
599 *Pharmacol.* **372**, 385–399 (2006).
600 42. W. R. Light, J. S. Olson, Transmembrane movement of heme. *J. Biol. Chem*. **265**, 15623–15631 (1990).
601 43. W. R. Light, J. S. Olson, The effects of lipid composition on the rate and extent of heme binding to membranes.
602 *J. Biol. Chem*. **265**, 15632–15637 (1990).
603 44. J. A. Olsen, A. Alam, J. Kowal, B. Stieger, K. P. Locher, Structure of the human lipid exporter ABCB4 in a lipid
604 environment. *Nat. Struct. Mol. Biol.* **27**, 62-70 (2020).
605 45. W. Mi, Y. Li, S. H. Yoon, R. K. Ernst, T. Walz, M. Liao, Structural basis of MsbA-mediated lipopolysaccharide
606 transport. *Nature* **549**, 233-237 (2017).
607 46. Y. Kim, J. Chen, Molecular structure of human P-glycoprotein in the ATP-bound, outward-facing
608 conformation. *Science* **359**, 915-919 (2018).
609 47. E. Lambert, A. R. Mehdipour, A. Schmidt, G. Hummer, C. Perez, Evidence for a trap-and-flip mechanism in a
610 proton-dependent lipid transporter. *Nat. Commun.* **13**, 1-13 (2022).
611 48. S. Zakrzewska, A. R. Mehdipour, V. N. Malviya, T. Nonaka, J. Koepke, C. Muenke, W. Hausner, G. Hummer, S.
612 Safarian, H. Michel, Inward-facing conformation of a multidrug resistance MATE family transporter. *Proc. Natl.*
613 *Acad. Sci. U.S.A.* **116**, 12275–12284 (2019).
614 49. S. Hofmann, D. Januliene, A. R. Mehdipour, C. Thomas, E. Stefan, S. Brüchert, B. T. Kuhn, E. R. Geertsma, G.
615 Hummer, R. Tampe, A. Moeller, Conformation space of a heterodimeric ABC exporter under turnover conditions.
616 *Nature* **571**, 580-583 (2019).
617 50. J.-S. Woo, A. Zeltina, B. A. Goetz, K. P. Locher, X-ray structure of the Yersinia pestis heme transporter HmuUV.
618 *Nat. Struct. Mol. Biol*. **19**, 1310–1315 (2012).

619 51. D. L. Mendez, E. P. Lowder, D. E. Tillman, M. C. Sutherland, A. L. Collier, M. J. Rau, J. A. J. Fitzpatrick, R. G.
620 Kranz, Cryo-EM of CcsBA reveals the basis for cytochrome c biogenesis and heme transport. *Nat. Chem. Biol*. **18**,
621 101–108 (2022).
622 52. H. Nakamura, T. Hisano, Md. M. Rahman, T. Tosha, M. Shirouzu, Y. Shiro, Structural basis for heme
623 detoxification by an ATP-binding cassette–type efflux pump in gram-positive pathogenic bacteria. *Proc. Natl.*
624 *Acad. Sci. U.S.A.* **119**, e2123385119 (2022).
625 53. Y. Naoe, N. Nakamura, A. Doi, M. Sawabe, H. Nakamura, Y. Shiro, H. Sugimoto, Crystal structure of bacterial
626 haem importer complex in the inward-facing conformation. *Nat. Commun*. **7**, 13411 (2016).
627 54. F. M. Arnold, M. S. Weber, I. Gonda, M. J. Gallenito, S. Adenau, P. Egloff, I. Zimmermann, C. A. J. Hutter, L. M.
628 Hürlimann, E. Peters, J. Piel, G. Meloni, O. Medalia, M. A. Seeger, The ABC exporter IrtAB imports and reduces
629 mycobacterial siderophores. *Nature* **580**, 413–417 (2020).
630 55. M. D. Esposti, T. Rosas-Pérez, L. E. Servín-Garcidueñas, L. M. Bolãnos, M. Rosenblueth, E. Marťınez-Romero,
631 Molecular Evolution of Cytochrome bd Oxidases across Proteobacterial Genomes. *Genome Biol. Evol.* **7**, 801-820
632 (2015).
633 56. L. Shi, C. D. Sohaskey, B. D. Kana, S. Dawes, R. J. North, V. Mizrahi, M. L. Gennaro, Changes in energy
634 metabolism of Mycobacterium tuberculosis in mouse lung and under in vitro conditions affecting aerobic
635 respiration. *Proc. Natl. Acad. Sci. U.S.A.* **102**, 15629-15634 (2005).
636 57. Q. L. Truong, Y. Cho, S. Park, K. Kim, T.-W. Hahn, Brucella abortusΔcydCΔcydD and ΔcydCΔpurD double-
637 mutants are highly attenuated and confer long-term protective immunity against virulent Brucella abortus.
638 *Vaccine* **34**, 237–244 (2016).
639 58. A. Moosa, D. A. Lamprecht, K. Arora, C. E. I. Barry, H. L. M. Boshoff, T. R. Ioerger, A. J. C. Steyn, V. Mizrahi, D.
640 F. Warner, Susceptibility of Mycobacterium tuberculosis Cytochrome bd Oxidase Mutants to Compounds
641 Targeting the Terminal Respiratory Oxidase, Cytochrome c. *Antimicrob. Agents Chemother.* **61**, e01338-17
642 (2017).
643 59. N. Dhar, J. D. McKinney, Mycobacterium tuberculosis persistence mutants identified by screening in isoniazid-
644 treated mice. *Proc. Natl. Acad. Sci. U.S.A.* **107**, 12275–12280 (2010).
645 60. M. Shepherd, M. D. Heath, R. K. Poole, NikA binds heme: A new role for an Escherichia coli periplasmic nickel-
646 binding protein. *Biochemistry* **46**, 5030-5037 (2007).
647 61. J. Dresler, J. Klimentova, J. Stulik, Francisella tularensis membrane complexome by blue native/SDS-PAGE. *J*
648 *Proteomics* **75**, 257–269 (2011).
649

650 **Acknowledgements**
651 We thank Alexander Hahn and Gregory Cook for valuable discussions. We thank Hartmut Michel for support
652 and providing infrastructural resources.
653
654
655 **Funding**

This work was supported by the Max Planck Society and the Nobel Laureate Fellowship of the Max Planck Society.

Author contributions

D.W purified CydDC, prepared grids, collected cryo-EM data, processed cryo-EM data, refined the structure, built the model, co-drafted the manuscript, and prepared figures. F.F purified CydDC, prepared grids, collected cryo-EM data, performed biochemical activity assays, analyzed data, and drafted figures. H.G.G performed bacterial growth assays, determined oxygen consumption rates, and collected UV-Vis spectra. A.R.M performed MD simulations, co-drafted the manuscript, and prepared figures. T.N.G performed biochemical activity assays and analyzed data. R.G optimized purification conditions and performed initial cryo-EM screening experiments. T.R implemented purification and optimized CydDC buffer conditions. R.Z assisted in cell culturing and protein purification. M.S provided p*cydDC* and p*H85A*, and established the enzyme coupled ATPase assay. S.W calibrated and aligned the microscope. M.S and S.S initiated the project. G.H, D.B, M.S, and S.S supervised the project. S.S designed research, evaluated data, funded the project, drafted the manuscript, and generated figures.

Data availability

Cryo-EM maps are deposited at the Electron Microscopy Data Bank under accession numbers: EMD-14636, EMD-14638, EMD-14639, EMD-14640, EMD-14641, EMD-14642, EMD-14643, EMD-14644, EMD-14645, EMD-14646, EMD-14647, EMD-14649, EMD-14652, EMD-14653, EMD-14654, EMD-14655, EMD-14656, EMD-14657, EMD-14659, EMD-14660, EMD-14662, EMD-14663, EMD-14665, EMD-14667, EMD-14668, EMD-14669, EMD-14670, EMD-14671, EMD-14672, EMD-14673, EMD-14674, EMD-14675, EMD-14676, EMD-14684, EMD-14689, EMD-15264, EMD-15265. Atomic models of CydDC have been deposited to the Protein Data Bank under accession numbers: 7ZD5, 7ZDA, 7ZDB, 7ZDC, 7ZDE, 7ZDF, 7ZDG, 7ZDK, 7ZDL, 7ZDR, 7ZDS, 7ZDT, 7ZDU, 7ZDV, 7ZDW, 7ZE5, 7ZEC. All other data is presented in the main text or supplementary materials. Source data are provided with this paper.

Competing interests

The authors declare no conflict-of-interest.

Figures

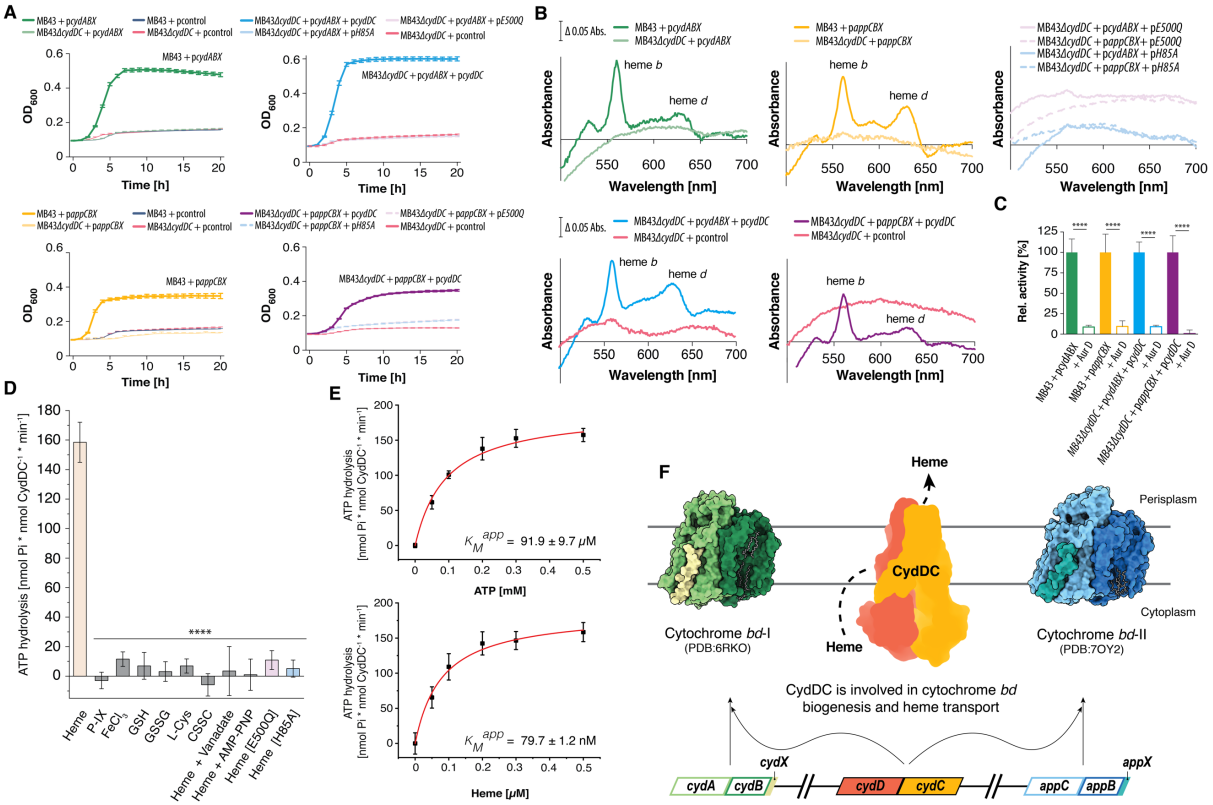

Fig. 1 – Physiological and biochemical links between CydDC activity and cytochrome *bd* biogenesis. (A) Growth complementation studies using *E. coli* MB43 and MB43*Δcyd*DC. Both strains lack NADH dehydrogenase I and all terminal oxidases. Cytochrome *bd* variants: p*cydABX* – wild-type cyt. *bd*-I; p*appCBX* – wild-type cyt. *bd*-II. CydDC variants: p*cydDC* – wild-type variant; p*E500Q* – glutamate to glutamine exchange at position 500 of CydC; p*H85A* – histidine to alanine exchange at position 85 of CydC. Control plasmid: pcontrol – empty pET17 vector. **(B)** Reduced-minus-oxidized UV-Vis spectra (450 - 700 nm) of membrane fractions from strains with restored/impaired growth phenotypes. Peaks corresponding to *b*-type and *d*-type hemes are indicated. **(C)** Oxygen reductase activity of membranes fractions from strains with growth-active phenotypes following complementation with structural genes of cytochrome *bd*-I, *bd*-II, and CydDC, respectively. Aurachin D (Aur. D) induced inhibition of oxygen consumption indicates for cytochrome *bd* specific oxygen reductase activity. Data are given as mean of n=3 ± SD. Significance was assessed based on a paired two-tailed Student's t-test (**** $p < 0.0001$). **(D)** ATP hydrolysis activity of CydDC in the presence of putative substrate molecules. Data are given as mean of n=3 ± SD. Significance was assessed based on a paired two-tailed Student's t-test (***, $p < 0.001$; ****, $p < 0.0001$). **(E)** Titration experiments for the determination of Michaelis constants (K_M^{app}) for ATP (91.9 ± 9.7 μM) and heme (79.7 ± 1.2 nM). All presented ATP hydrolysis data are corrected for background activity in the absence of substrate candidates. **(F)** Working model for substrate specificity and physiological role of CydDC based on independent physiological and biochemical data generated in this study.

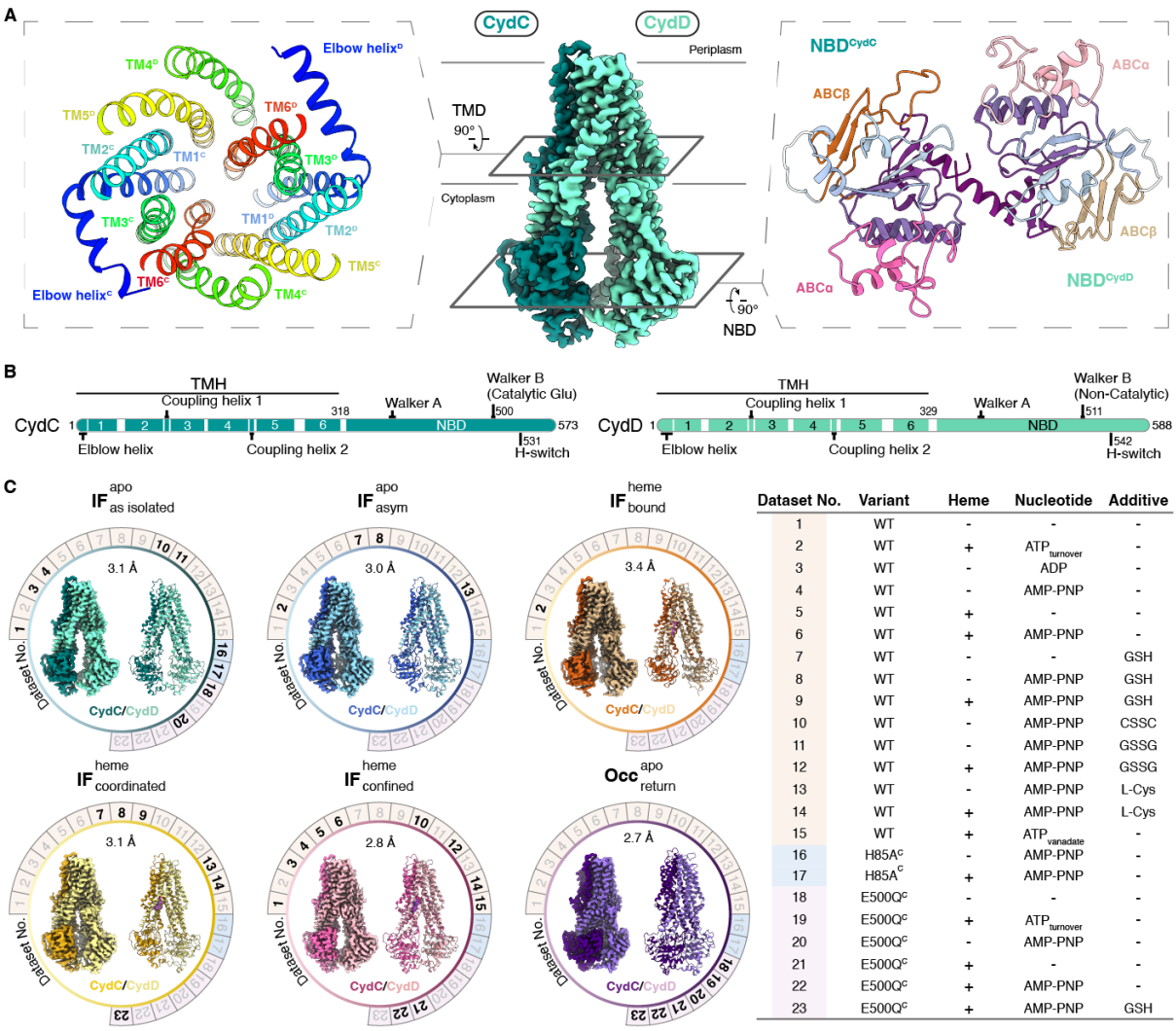

Dataset No.	Variant	Heme	Nucleotide	Additive
1	WT	-	-	-
2	WT	+	$ATP_{turnover}$	-
3	WT	-	ADP	-
4	WT	-	AMP-PNP	-
5	WT	+	-	-
6	WT	+	AMP-PNP	-
7	WT	-	-	GSH
8	WT	-	AMP-PNP	GSH
9	WT	+	AMP-PNP	GSH
10	WT	-	AMP-PNP	CSSC
11	WT	-	AMP-PNP	GSSG
12	WT	+	AMP-PNP	GSSG
13	WT	-	AMP-PNP	L-Cys
14	WT	+	AMP-PNP	L-Cys
15	WT	+	$ATP_{vanadate}$	-
16	$H85A^{C}$	-	AMP-PNP	-
17	$H85A^{C}$	+	AMP-PNP	-
18	$E500Q^{C}$	-	-	-
19	$E500Q^{C}$	+	$ATP_{turnover}$	-
20	$E500Q^{C}$	-	AMP-PNP	-
21	$E500Q^{C}$	+	-	-
22	$E500Q^{C}$	+	AMP-PNP	-
23	$E500Q^{C}$	+	AMP-PNP	GSH

Fig. 2 – Systematic cryo-EM approach. (A) Volume map representation of the $\mathbf{IF}^{\mathrm{heme}}_{\mathrm{as\ isolated}}$ structure representing the general architecture of CydDC. Dark green, CydC; light green, CydD. Left: cross-section of the membrane domain composed of 12 TMs showing arrangement and geometry typical for type IV ABC transporters. Right: cross-section of nucleotide-binding domains (NBDs). The subdomains ABCα and ABCβ of each NBD are highlighted. **(B)** Schematic organization of CydC and CydD subunits. TMs are indicated by numbers. Residues important for ATP hydrolysis and signal transduction between TMH and NB domains are highlighted. **(C)** Summary of systematic single-particle cryo-EM studies. Left: volume maps and corresponding ribbon models within each circle represent a distinct conformation of CydDC. Numbers around circles refer to sample condition of CydDC analyzed by electron microscopy. Bold numbers indicate that the given conformation was present under that condition. Right: summarized information about the analyzed CydDC variants, presence and absence of heme, nucleotide, and additional putative substrate molecules. $CydDC^{wt}$, beige; $CydDC^{H85A}$, light blue; $CydDC^{E500Q}$, purple. IF, inward-facing; Occ, occluded.

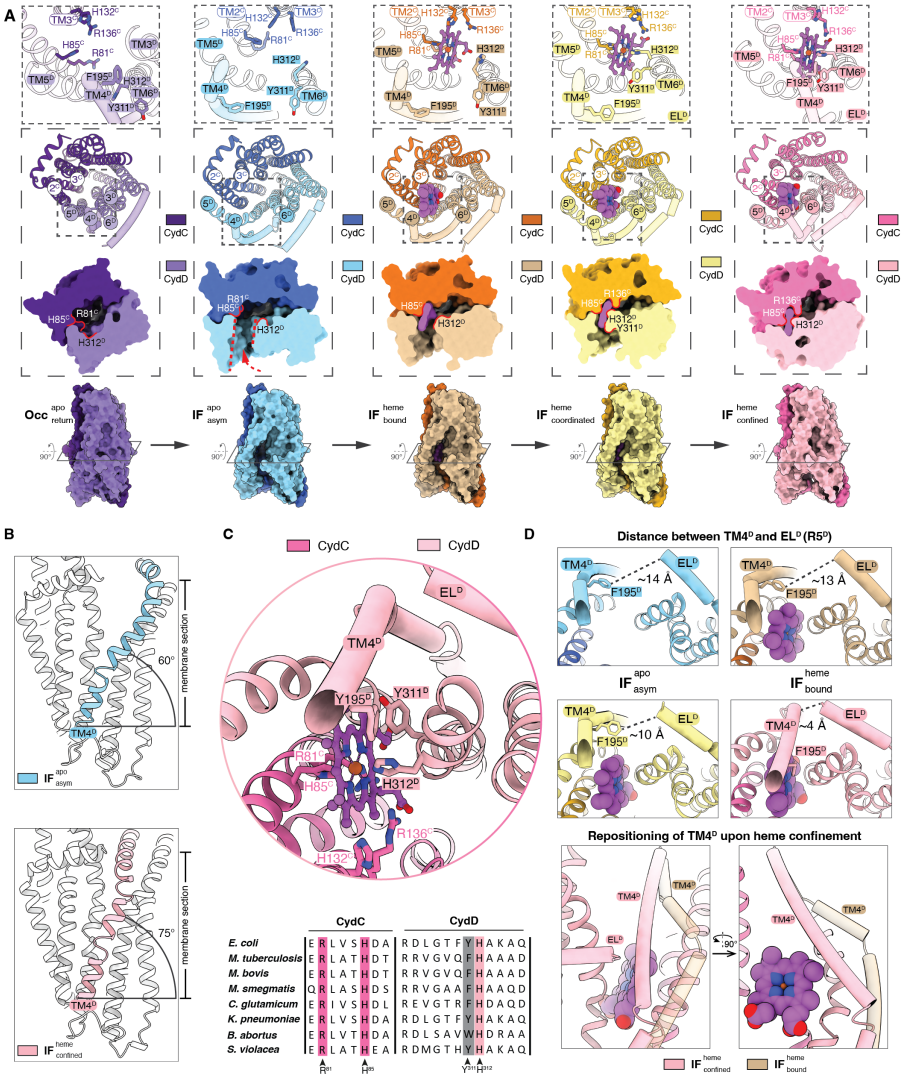

Fig. 3 – Conformational landscape of heme binding and translocation. (**A**) Closeup views show residues involved in heme binding and occlusion. Surface model cross sections illustrate the changing shape and size of the internal cavity in different conformational states. Surface model side views highlight the change in overall shape of the TMH region in different conformational states. Heme is shown as purple ball-and-stick model. EL1^{D} and TM4^{D} are shown as tubes. (**B**) Upon heme entry and coordination, the membrane-embedded segment TM4^{D} helix moves towards EL^{D} and thus closes the lateral gate of CydDC. **(C)** Top: closeup view of the heme binding site in the $\mathbf{IF}^{\mathrm{heme}}_{\mathrm{confined}}$ state. Heme is axially coordinated by two histidine residues (H85^{C} and H312^{D}). Propionate groups of the heme molecule form electrostatic interactions with invariant R81^{C} and R136^{C}. The heme macrocycle is further held in place by F195^{D} and Y311^{D}, which restrict lateral movement towards the membrane and act as internal gate-forming residues. Bottom: sequence alignments of CydD and CydC heme binding-site forming regions of representative and disease related bacteria. Conserved residues are highlighted in magenta. Conserved amino acid groups are highlighted in gray. **(D)** Top**:** changing EL^{D} - TM4^{D} distance during the transition from $\mathbf{IF}^{\mathrm{apo}}_{\mathrm{asym}}$ to $\mathbf{IF}^{\mathrm{heme}}_{\mathrm{confined}}$ states shown by ribbon models viewed from the cytoplasmic angle. Distances are indicated by dashed lines. Bottom: closeup view of the membrane-exposed and sealed heme entry site in $\mathbf{IF}^{\mathrm{heme}}_{\mathrm{bound}}$ (beige) and $\mathbf{IF}^{\mathrm{heme}}_{\mathrm{confined}}$ (magenta) states, respectively. During the transition from $\mathbf{IF}^{\mathrm{apo}}_{\mathrm{asym}}$ via $\mathbf{IF}^{\mathrm{heme}}_{\mathrm{bound}}$ to $\mathbf{IF}^{\mathrm{heme}}_{\mathrm{confined}}$ we observe that the cytoplasmic portion of TM4^{D} approaches the heme molecule and is positioned above it, contributing to substrate confinement. IF, inward-facing; OF, outward-facing; Occ, occluded; asym, asymmetrical.

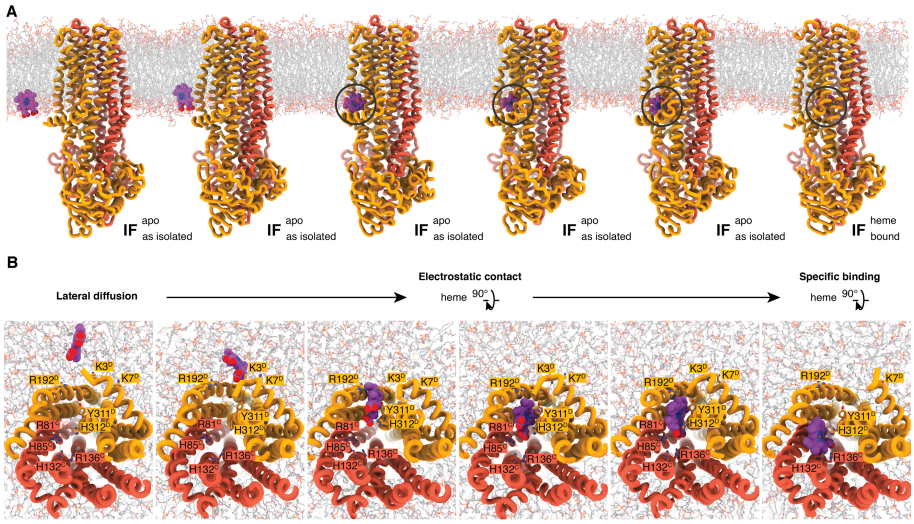

Fig. 4 – Structural dynamics of the heme binding and flipping mechanism. (A) Representative snapshots of MD simulations showing the lateral diffusion and entry of heme to the membrane-accessible binding cavity of CydDC. **(B)** Closeup views show that once heme interacts with the electrostatic surface and the interior of the binding cavity of CydDC, a 90° rotation occurs that orients the propionate groups of the porphyrin macrocycle horizontally. A second 90° rotation takes place upon bilateral axial coordination via H85^{C} and H312^{D}, which results in a complete flip of the heme molecule compared to its conformation when immersed freely within the lipid bilayer.

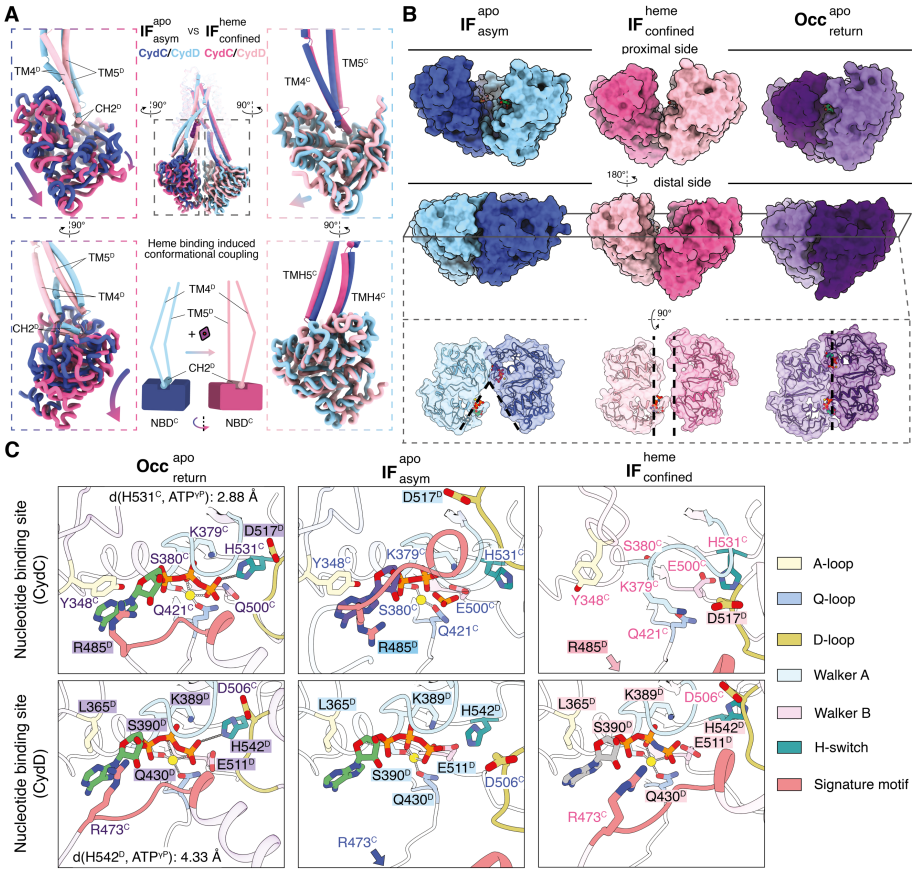

Fig. 5 – Signal transduction between TMH and NB domains. (A) Mechanism of conformational coupling between TMH and NB domains. Occlusion of the lateral substrate gate induces conformational changes of TMs 4 & 5 of CydD causing a rotational movement of NBD^C via coupling helix 2 ($CH2^D$). No conformational coupling between TMs of CydC and NBD^D is observable. Dark blue, CydC; light blue, CydD; dark pink, CydC; light pink, CydD. **(B)** Surface representation of NBD-NBD interactions in proximal and distal view. Cross section top view on the level of the nucleotide-binding sites (NBS) shows distinctly different NBD conformations. $\mathbf{IF}^{\mathrm{apo}}_{\mathrm{asym}}$, blue; $\mathbf{IF}^{\mathrm{heme}}_{\mathrm{confined}}$, magenta; $\mathbf{Occ}^{\mathrm{apo}}_{\mathrm{return}}$, purple. **(C)** Closeup view of nucleotide-binding pockets in different conformational states and nucleotide occupancies. Conserved structural motifs of the nucleotide-binding and hydrolysis sites are highlighted. ATP, green; ADP, purple; AMP-PNP, grey; phosphate, orange; Mg^{2+}, yellow.

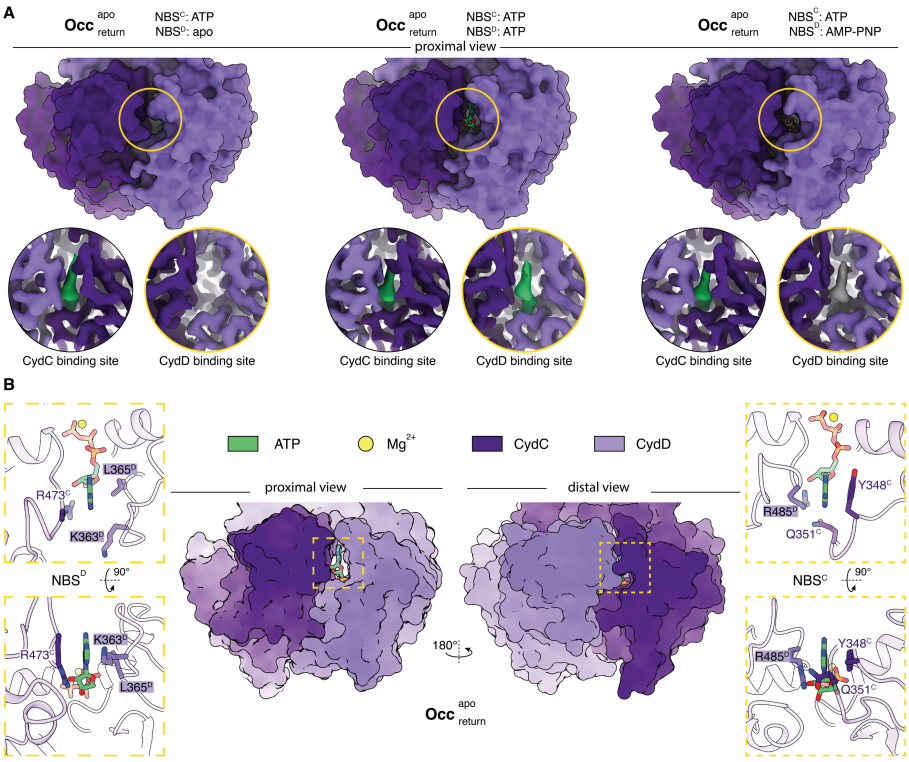

Fig. 6 – Local environment and accessibility of NBS^D and NBS^C. (A) Top panel**:** proximal view of tightly-interlocked NBDs in the $\mathbf{Occ}^{\mathrm{apo}}_{\mathrm{return}}$ state from CydDC^{E500Q} shown as surface models (datasets 17-19). Bottom panel: closeup views of the NBS regions of CydD and CydC show sample-condition specific differences in nucleotide occupancy. ATP densities are shown in green, AMP-PNP densities are shown in grey. Densities of CydD and CydC are shown in dark and light purple, respectively. Bound ATP at NBS^C is enclosed by tight interactions between the CydC A-loop and the ABCα region of CydD in adjacency of the adenine group. The corresponding loops at NBS^D are separated widely and expose ATP bound at this site to the solvent. **(B)** Center panel: surface model of the interlocked NBD dimer in the $\mathbf{Occ}^{\mathrm{apo}}_{\mathrm{return}}$ state from the turnover dataset of CydDC^{E500Q}. Left panel: closeup view of ATP bound to NBS^D in top and side view orientation. Residues forming the local protein environment close to the adenine head group are shown. Right panel: closeup view of ATP bound to NBS^C in top and side view orientation. Residues forming the local protein environment close to the adenine head group are shown. ATP, green; Mg^{2+}, yellow; CydC, light purple; CydD, dark purple.